Research Square

Preprints are preliminary reports that have not undergone peer review.
They should not be considered conclusive, used to inform clinical practice,
or referenced by the media as validated information.

Multi-layer silicon nanoparticle solar cells: Conceptual design and performance analysis

Sayyed Reza Mirnaziry
University of Tehran, Science and Technology Park
Mohammad Ali Shameli
University of Tehran
Leila Yousefi (lyousefi@ut.ac.ir)
University of Tehran

Article

Keywords:

Posted Date: April 14th, 2022

DOI: https://doi.org/10.21203/rs.3.rs-1542902/v1

License: This work is licensed under a Creative Commons Attribution 4.0 International License.
Read Full License

Multi-layer silicon nanoparticle solar cells: Conceptual design and performance analysis

Sayyed Reza Mirnaziry[1], Mohammad Ali Shameli[2], and Leila Yousefi[2,*]

[1]University of Tehran, Science and Technology Park, Tehran, 1417466191, Iran
[2]School of Electrical and Computer Engineering, College of engineering, University of Tehran, Tehran, 1417614411, Iran
[*]lyousefi@ut.ac.ir

ABSTRACT

We investigate the concept of nanoparticle-based solar cells composed of a silicon nanoparticle stack acting as efficient light trapping absorbers to achieve novel inorganic configurations for ultrathin photovoltaics. We study the potential of using these inherently nanotextured structures in enhancing the light absorption. For this, a detailed optical analysis is performed to demonstrate the dependency of the typical structure to physical parameters including the number of particle layers, lattice structure and angle of incidence; these behavior are then compared with conventional silicon solar cells. We propose various configurations to apply these sub-micron particles as a p-n junction solar cell. We also compute the electrical performance of selected configurations. In doing so, key issues including the effect of contact points between nanoparticles and impact of loss are addressed. In the end, we show how SiO_2 nanoparticles on top of the cell structure can enhance the photocurrent. The appropriate range of SiO_2 particle size is also obtained for the typical cell structures.

Introduction

Ultrathin solar cells are generally referred to a group of photovoltaic structures possessing light absorbers with a thickness of at least an order of magnitude smaller than conventional solar cells. Despite their reduced thickness, the optical path length is increased considerably by engineering the cell structure so as to compensate the likely low absorption. In this regard, not only the material thickness but primarily material selection, doping, top and back contacts must be properly chosen. In terms of advantages, ultrathin solar cells are attractive for decreasing the raw material requirements, flexibility and bendability[1,2]; In addition, they are expected to be fabricated with low-cost techniques via increased fabrication throughput[3]; for instance, they may be realized without protective glass layers[2] or their active layer can be deposited with lower deposition techniques[4]. These cells can show robust performance in cell dislocations and low light-induced degradation[5,6]. Besides, bulk recombination mechanisms such as Auger recombination - are limited, which result in higher open-circuit voltages, and carrier collection is facilitated on contacts[4]. The concept of ultrathin photovoltaics has experienced a fascinating growth through the last decade as it found applications in spacecrafts[2] due to their short carrier diffusion lengths, which brings immunity against radiation damages. In addition, due to their flexibility, these cells are promising as energy supply for portable devices in remote areas.

Attempts for design and realization of ultrathin solar cells has been concentrated on studying both the electrical and optical aspects; On the electrical side, common analysis include optimization of cell absorbers bandgap[7,8], together with studying photo-carrier drift, diffusion, generation and recombination using the transport equations[9,10]. In terms of optical side, the absorption behavior of a cell is the key parameter that determine how efficient a cell architecture act to produce higher photocurrent. Regarding the ultrathin structures the main drawback for reaching high efficiencies is insufficient light absorption - in comparison to conventional cells. Due to this, researches on these cells are often directed toward finding light management architectures with practical values[6,11–14]. For instance, using proper anti-reflection coatings and embedding back mirrors[15,16], using periodic nano-gratings on the front[17–19], or random pyramids on the front and back of ultrathin silicon layers to achieve omnidirectional reflectance[20]. Optical confinement has also been explored through the excitation of edge states around the photonic topological insulator[21]. Considering these, the attempt has therefore been focused on configuring the structure both optically and electrically to preserve high short circuit currents while decreasing the thickness.

The reported efficiencies for ultrathin solar cells are promising; In GaAs cells of thickness around 205 nm, a 19.9% efficiency is obtained[2], which is competitive with the values extracted for conventional cells; In terms of Si solar cells, the efficiency of 8.6% is reached for a 1.1 um absorber, that although lower than its traditional counterparts - due to the intrinsic low absorption of silicon at higher wavelengths - it is considered a remarkable progress for cells based on this commercially available material[4]. For CIGSe cells with the thickness of 1.2 um, the efficiency of 11.27% is reported in[22].

Pattering an ultrathin structure can, however, complicate the realization of these cells and even contradict with their principle benefits. Thus, simple cell configurations with reasonable efficiencies are most often preferred. Among various techniques to increase the short circuit current in ultrathin cells, using randomly roughened surfaces has shown promising results[6]. In this regard, the beneficial effect of nanoparticles on absorption enhancement and broadening solar spectral band for ever thinner solar cells has been extensively addressed[23–26]; In terms of fabrication, in contrast to photonic crystal patterns, nanoparticles can be made and deposited via lower cost techniques[27]. While the attentions on ultrathin solar cells have been mainly drawn toward GaAs solar cells (see for instance[28]), the low cost silicon solar cells of this type possess commercially more chance to be employed in widespread terrestrial applications with low energy requirements.

In this paper, we demonstrate multi-layer Silicon Nano-Particle (SNP) solar cells as a promising photon management technique in ultrathin photovoltaics. We show how this inherently textured architecture acts as a light absorber while having the potential to separate and transport photo-generated carriers. We compare the optical properties of a structure composed of these Mie scatterers with planar cells of the same thickness and provide a comprehensive analysis on the cell behavior for different number of particle layers when exposed to oblique incidence and also for various particle periodicity. Then, we study different scenarios to tailor the silicon nanoparticles as the active layer of a realizable cell. Next, we concentrate on an appropriate structure and optimize its geometrical and electrical parameters. In order to further improve the absorption, we examine the effect of distributing SiO_2 nanoparticles on the cell front. Finally, we estimate the expected power conversion efficiency of the cell and compare it with the efficiencies reported in the literature.

Electromagnetic properties of multi-layer SNP absorbers

Conventional silicon solar cells absorb sunlight in the bulk of the active layer, however away from the surface, major volume of this expensive layer does not receive considerable amount of light, hence mostly acts as a carrier transporting medium. To address this, various techniques have been proposed for thin-film solar cells. One interesting idea - that establishes the core of this study - is to replace the silicon layer with an architecture composed of multi-layer silicon nanoparticles. As shown in Fig.1a, the silicon nanoparticles are densely stacked into a host dielectric medium. This configuration is compared with a flat silicon layer on a metallic electrode (Fig.1b). We assume that particles have an identical size of the order of a few hundred nanometers; this dimension range ensures achieving a remarkable light trapping through the frequency spectrum which contributes in photo-generation (i.e. $\lambda = 300 - 1100\,\text{nm}$). Assuming the spherical shape of silicon nanoparticles, by reducing the particle radius, a lower number of Mie resonances are excited and this leads to a lower light absorption. In addition, we will see that as the particle radius approaches around 500 nm and above, the absorption enhancement - in comparison to a conventional cell - becomes negligible. This is because the absorption for the silicon nanospheres with a radius of 500 nm or larger will be close to the unity in the bandwidth of the solar cells. Light trapping in this particle-based structure is enhanced due to the excitation of whispering gallery modes. Moreover, from the ray optics viewpoint, the random path length of light beams inside the structure increases total absorption. With regard to the flat silicon layer shown in Fig.1b, at $\lambda < 500\,\text{nm}$, the absorption is due to the intrinsic loss of the crystalline silicon. In this range, thus the optical responses of both structures are very close together. At higher wavelengths, the Fabry-Perot resonance is the only mechanism for trapping light in the flat structure, and it happens only at a few wavelengths. In the following sections, we examine various aspects of distributed silicon nanoparticles in light

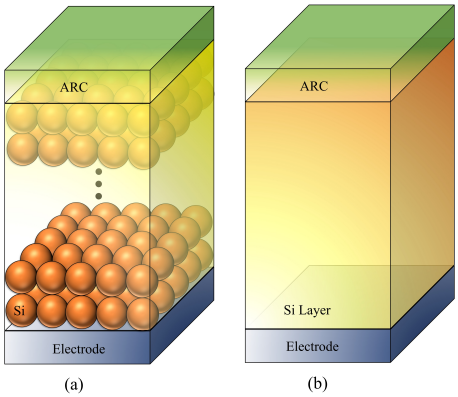

Figure 1. (a) The schematic of a structure composed of identical silicon nanoparticles arranged to form a dense periodic structure. On the top, there exist an anti-reflection coating (ARC). This structure is compared - in terms of absorption - with a configuration shown in (b) wherein, particles are replaced by a silicon layer of an identical thickness.

absorption, if they are employed instead of the silicon layer.

Comparison in terms of the number of layers

To study the effect of the number of layers in Fig.1a, and compare its optical response with a silicon layer of equal thickness shown in Fig.1b, we computed the absorption of both structures at the interested frequency interval using CST (Details of simulation methodology are explained in the last section). We assume that particles are spherical with a selected radius of 300 nm. Particles are assumed to be inside a carrier transport medium with the refractive index of 1.8, which is a average value for a number of materials such as PEDOT:PSS polymer and SPIRO-OMETAD at the interested frequency spectrum of sunlight. The thickness of this medium above the upper layer is assumed to be 75 nm, which imitates the typical thickness of an ARC. Figure 2a and b show the absorption spectra of a multi-layer SNP absorber with two (N = 2) and five (N = 5) layers of silicon nanospheres when compared with that of a flat layer (By integrating the obtained graphs over the wavelength interval, we can compute the sunlight power density that is absorbed by the structure). As can be seen, a particle-based structure and a flat layer behave the same at short wavelengths in both figures. This was expected as the penetration depth is such small that the optical power is absorbed regardless of the considered configuration change. However, these particle-based structures provide improved absorption, at longer wavelengths. Moreover, by comparing the two figures, higher absorption is achieved when N = 5. Note that, if we assumed that the two structure (i.e. the multi-layer SNP and a flat structure) should have identical absorber volume, we would reach even further discrepancy in their absorption at long wavelengths.

Although the absorption is enhanced as the number of layers increases, the total absorption approaches that of a planar structure. This is shown in Fig. 2c where the total absorbed power density - at the interested wavelength interval - is computed for the particle-based structure and the planar one, as a function of the number of layers. We have also defined the total absorption enhancement as ratio between the total absorbed power density of the two structure. From the figure, using a large number of SNP layers dose not provide an advantage compared to planar structure. This indicates that a SNP solar cell is preferable only when a few layer is used.

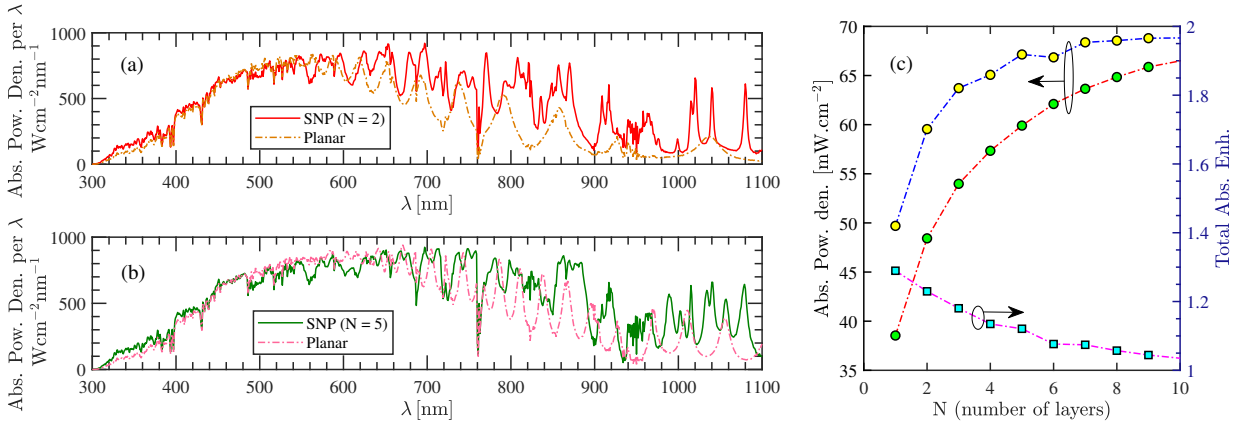

Figure 2. The absorbed power density per wavelength of a multi-layer SNP cell with (a) N = 2 and (b) N = 5 particle layers in the presence of solar irradiance. Silicon particles are spherical with the radius of 300 nm. The results are compared with the absorption of a silicon layer of the same thickness in both SNP cells (the dotted-dashed lines). (c) shows the total absorbed power density of the structure shown in Fig.1a, as a function of the number of particle layers. The absorption enhancement from a silicon layer is also depicted in the figure.

Comparison in terms of lattice type

Particles in each layer of the structure shown in Fig.1a may be arranged in different forms. Considering a dense distribution, a random arrangement for particles is a cheaper choice and practically preferred one for mass production. Despite this, in terms of numerical analysis, one often has to consider a sort of periodicity to reduce the simulation domain. Knowing the impact of various particle distributions on the absorption behavior helps in finding an average expected response of a random distribution. Before studying the impact of particle arrangements, we emphasize that dense distributions are much more desirable than sparse ones for solar cell applications. This is because silicon nanoparticles form the main cell absorber and thus, any distance between them leads to a drop in absorption of incident photons. Also, as the nanoparticles become closer, a stronger coupling will be formed inside the solar cell.

We restrict our study to a lattice composed of two layers of identical silicon nanoparticles with radius R. Figure 3 shows the cross-sectional top-view of three different arrangements of these layers. In Fig.3a, particles in each layer are assumed

to form a rectangular lattice where the distance between particle centers along each x and y direction is 2R. Moreover, the cross-sectional location of particle centers in the upper layer reside on the particle centers in the lower layer. In Fig.3b, the upper layer - shown inside the dashed square has a rectangular cross-section and - is shifted with a lattice vector $R\hat{a}_x + R\hat{a}_y$ with respect to its below layer. Finally in Fig.3c, each layer has a hexagonal lattice in the 2D cross-section, with an upper layer having the same pattern placed exactly on the location of lower particles. The reflection of these three structures are compared for (R = 100 nm) in Fig.3d. As can be seen, the reflection from the first and third arrangements have very similar behavior at lower wavelengths; at higher wavelengths, the hexagonal structure has an improved absorption due to its new resonances. The reflection corresponding to the second lattice presents a fairly fluctuating behavior; while the reflection is reduced in several wavelength intervals, between 680 and 780 nm, it is increased. The total reflection from these structures is also shown in the figure. Moreover, the photocurrent produced by each one is obtained via[29]

$$J_{\text{ph}} = \frac{e}{hc}\int_{\lambda=300\text{nm}}^{\lambda=1100\text{nm}} S(\lambda)A(\lambda)\lambda d\lambda, \tag{1}$$

where c is the speed of light, e is the electron charge, h is Planck's constant, and $S(\lambda)$ is AM 1.5G solar spectrum[30]. The values show that the second form of periodicity - which much more resembles a quasi-random distribution - can generate larger values of current. Despite this, we consider the worst scenario (i.e. the first form of periodicity) when simulating the electrical behavior of these structures.

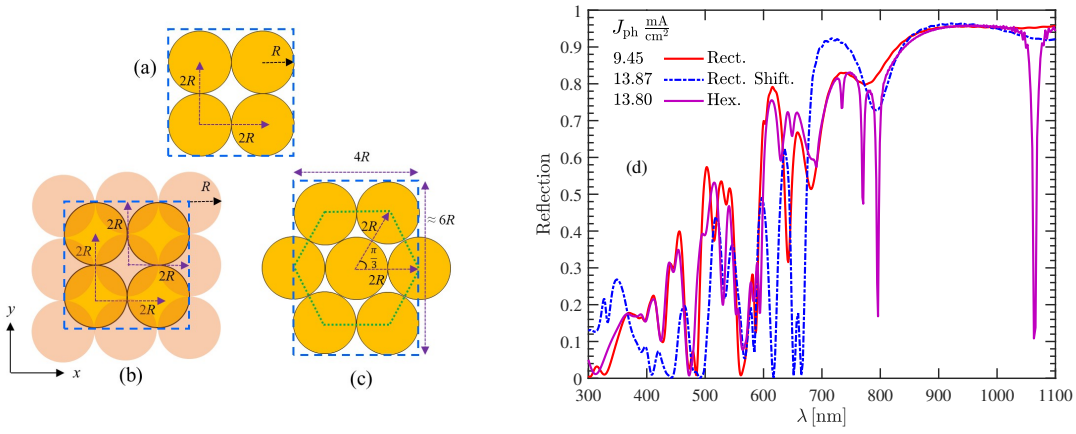

Figure 3. Three forms of lattice arrangement for the silicon particles in the multi-layer structure shown in Fig.1. (a), (b) and (c) show the cross-section of the structure from its top view. In (a), particles of identical size in each layer are exactly located on top of their below particles. In (b), each upper particle fills the gaps between four lower particles. In (c), each layer has a hexagonal lattice and the upper particles are exactly located below another particle with identical size. (d) Reflection from the various arrangement of the silicon nanoparticles in a dielectric medium with the refractive index of 1.8.

Comparison of the reflection influenced by the angles of incident

In this section, we investigate the dependency of Fig.1a to the angles of the incidence. Likewise the previous section, we concentrate on a SNP structure composed of a two-layer absorber covered by a dielectric medium with the thickness 50nm and refractive index of 1.8 (This layer is included to mimic the TCO layer in a real thin-film cell), and compute the absorption coefficient A at four different angles of incident $\theta = 15^\circ$, 30°, 45° and 60° through the interested spectrum. The results are shown in Fig.4(a-d). In addition, the absorption of the particle-based structure at each angle is compared with a flat silicon layer of equal thickness through the spectrum. As can be seen, the absorption of the multilayered particles does not seriously change at $\lambda > 600\,\text{nm}$. In contrast, at lower wavelengths, $\mathscr{A}$ experiences a noticeable reduction, particularly at $\theta = 45^\circ$ and 60°. This can be explained using the ray-optic point of view; as the incident beam hits obliquely on the top particles, only a little portion of top the surface belonging to the upper particles has this chance to interact with light. This is in contrast to the normal incidence, where the whole surface receives light. In a similar way, one can argue about the negligible angle-dependence of the flat structure through the whole spectrum. However, by computing the photocurrent due to the absorption in both structures, it reveals that at the angle $\theta = 60^\circ$ the SNP structure still provides higher $J_{\text{ph}}(27.8\text{mA}/\text{cm}^2)$ than the flat absorber $(21.6\text{mA}/\text{cm}^2)$. This implies that despite the reduction in the absorption efficiency, a SNP absorber is preferred to a flat one.

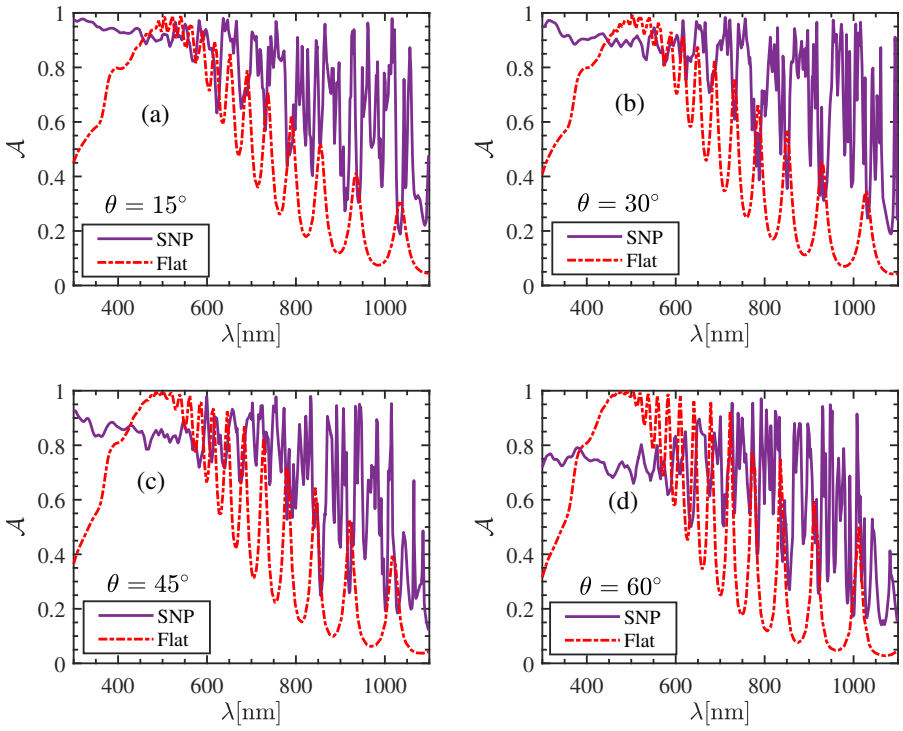

Figure 4. Impact of the angle of incidence on total absorption of a SNP structure composed of two layers of silicon nanoparticles with the dielectric medium with refracive index of 1.8 and thickness of 50 nm as a cover layer, all on a silver layer(The solid purple lines). Nanoparticles are identical spheres with the radius of 300 nm. The angles of incidents are (a) 15° (b) 30° (c) 45° and (d) 60°. The absorption spectrum in each case is compared with a flat silicon layer of the same thickness (the red dashed lines).

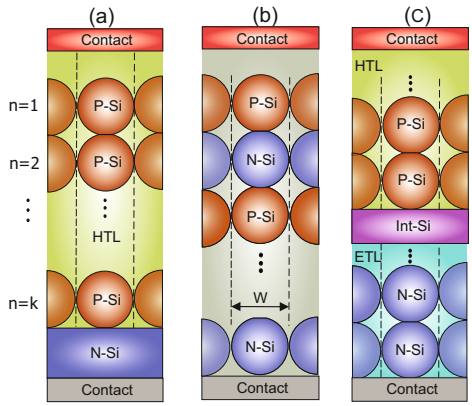

Figure 5. The schematics of a multi-layer SNP cell proposed to realize a thin solar cell using silicon nanoparticles. (a) k layers of p-doped silicon nanoparticles inside a hole transport layer are placed on a thin n-doped silicon layer. The dashed lines show the unit cell. (b) There is no silicon layer in the structure and doping of each particle layer differs from its adjacent layers. (c) Particles of opposite doping are separated via a thin intrinsic silicon layer.

Cell configurations and operating mechanism

Various configurations of ultrathin solar cells can be theoretically considered to operate based on silicon nanoparticles acting as absorbers. Depending on the particles size, its distribution (i.e. periodic or random) and the operating mechanism designed

for the cell, these structures can be categorized. As mentioned in the previous sections, silicon particles are assumed to have submicrion dimensions. However, cells based on silicon quantum dots are not considered here as poor carrier conductivity is still a serious drawback toward using them in photovoltaics[31]. With that in mind, in interested particles - with a few hundreds of nanometer dimensions - the particle band gap remains unchanged.

In terms of cell mechanism, we focus on configurations having p-n junctions. Depending on materials used as a host of nanoparticles there exists other quasi-p-n schemes that may be occur in the proposed cell structure; they will be discussed in the next sections. Figure 5 shows the cross-section of three cell configurations where particles have formed several layers and periodic structures. In our analysis we assume that particles have spherical shape to propose the main ideas and also for simulation considerations. However, in practice, nanoparticles may take random shapes when commercially produced[32] (This can apply slight changes in both optical and electrical analysis). Figure 5a shows a unit cell composed of several layers of doped silicon particles inside a dielectric medium. The p-doped particles are placed on a n-doped silicon layer to form a p-n junction. In this sense, the carrier transport toward contacts needs to occur through the particle interfaces. Therefore and theoretically, the surrounding medium for nanoparticles can be assumed to be air. However, for the stability reasons this is not a practical idea. Instead, assuming that silicon particles are p-type, then their surrounding medium can be filled by a hole transport material. This structure is then, a generalized form of the ultrathin structure proposed in[33]. The second structure shown in Fig. 5b is composed of merely multi-layers of silicon particles and form a multi p-n junction cell inside a dielectric medium. Each layer has particles with a doping that is opposite to its adjacent layers. The main concern about this configuration is that particles in upper layers may in practice diffuse into their below layers and hence, disrupt the expected carrier separation and transporting toward cell contacts. An alternative to realize a structure with particles of various doping, is the configuration shown in Fig.5c . As seen, particle layers of different doping are separated with a thin interlayer medium. This layer can be of intrinsic silicon. In practice, this ultrathin layer may be realized using even smaller silicon nanoparticles. The P(N)-doped silicon particles in this case are surrounded by a hole(electron) transport medium. A disadvantage of this structure is that particles below the intermediate layer do not effectively contribute in light confinement. However, the structure allows particles with various doping to form a cell structure. In the following we focus on the first structure and explore its optical and electrical parameters in a case study. Next, we look at the third structure and perform similar analysis to extract its electrical performance.

Structure A

The structure to be studied in this section is an example of the first cell topology proposed in the previous section. As shown in Fig.6a, the unit cell is composed of two p-doped silicon nanoparticles immersed in a HTL, which are placed above a N-doped silicon layer. We have also assumed that there exists an identical contact area between the nanoparticles. The HTL is assumed to be the organic polymer PEDOT:PSS in this case study, and has covered the particles with the thickness d_{HTL}. We note that solutions composed of silicon nanocrystals in polymers have been recently demonstrated for cheap and flexible optoelectronic applications[34]. Main material specifications and geometrical parameters of our case study are brought in Table 1.

Considering the dimensions given in the table, Fig.6b compares the photocurrent J_{ph} generated by the cell as a function of particle dimensions (All particles have identical size). These results are compared with the produced current a conventional silicon cell having identical thickness to the particle-based structure (i.e. Thickness = $d_{HTL} + d_{N-Si} + d_{P-Si}$). As can be seen, the proposed cell offers approximately 30% higher photocurrent in comparison to the flat cell. Thus, despite having less volume of absorber, the particle-based cell acts highly efficient for light trapping. As the particle dimension increases, the photocurrent takes naturally higher values. However, if we draw the ratio of photocurrent to the silicon volume used (see Fig.6c), we observe a downward trend with increasing the particle dimension, that indicates cell is becoming less efficient in terms of the absorber material consumed. Figure 6d shows the distribution of the carrier generation rate - in a logarithmic scale - of the cell in its cross-section. The generation rate is higher in the upper silicon particle; it is also highly concentrated in the bulk of the particles rather than the their boundaries. The current/power-voltage characteristics of the cell is obtained for various dopings of silicon layer in Fig.6e. As can be seen, by increasing the doping value, the open circuit voltage also improves.This is because the dark saturation current density is decreased by increasing doping. This improves the cell efficiency from 5.8% for $N_d = 10^{15}cm^{-3}$, to about 11% for $N_d = 10^{18}cm^{-3}$. Despite this, the short circuit current remains almost unchanged with doping variation. Figure 6f shows the distribution of total current density at V = 0.41 v when $N_d = 10^{18}cm^{-3}$. In addition, arrows show the direction of the normalized current density in the structure cross-section. As can be seen, particle contacts critically high densities - up to 120 $\frac{mA}{cm^2}$; at the top surface of the upper particle the current is much distributed with slightly higher values around highest point.

In practice, particles are hardly pure spherical. As a result, contacts between particles is an area rather than a single point. To consider this in modelings, we assume that the upper and below area of each particle are cropped. This forms a circular contact area as shown in Fig.7. We note that in extracting the I-V characteristics we have assumed that the contact area on upper and lower part of the nanoparticles has the radius $r_{cont.} = 60nm$. As we reduce this interface, the cell efficiency will be reduced. Table 2 shows the variation of the efficiency, short circuit and open circuit voltage as a function of $r_{cont.}$.

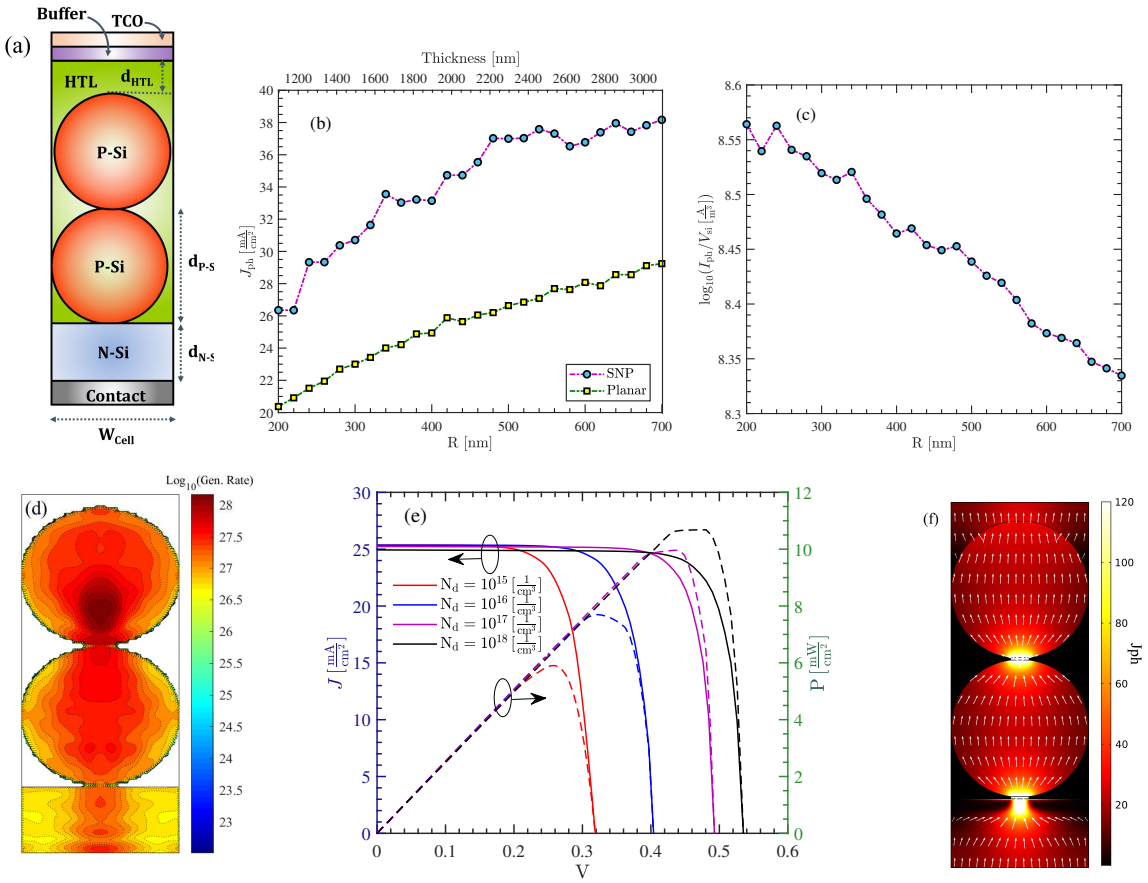

Figure 6. The schematic of the unit cell composed of two p-doped silicon nanoparticles inside a HTL materials that are placed on a n-doped silicon layer. The dimensions are listed in Tab1. (b) The photocurrent generated in structure shown in (a), and a conventional cell of identical thickness, as a function of particle size/absorber thickness. (c) The generated current per volume of the absorber for the cell shown in (a), as a function of particle radius. (d) The distribution of the generation rate in the cross-section of the unit cell in a logarithmic representation (unit is in m^{-3}). (e) J-V characteristics of the cell in (a), as a function of doping level of the silicon layer. The electrical parameters of the cell materials are brought in Tab1. (f) The total current density at V = 0.41 v, Arrows show the direction and distribution of the normalized current density in $\frac{mA}{cm^2}$.

Structure B

The second cell configuration is shown in Fig.8a wherein, two nanoparticles with various doping are deposited on the upper and lower sides of an intrinsic silicon layer. The geometrical parameters together with the used ETL properties are listed in Tab.3. Note that the HTL is similar to the structure illustrated in the previous section. Figure 8b shows the photocurrent generated in the cell structure as a function of silicon particle size; the results are also compared with a conventional cell of the same thickness. A similar behavior to the previous case study can be seen for both cell structures (i.e. particle-based cell and conventional one). In terms of current produced per volume of the unit cell, Fig.8c shows that smaller particles are more efficient despite generating lower levels of photocurrent. The generation rate of the unit cell over the cross section in Fig.8d shows that most carriers are generated at upper nanoparticle and the generation rate reaches $10^{28}\frac{1}{s.cm^3}$ around the particle center. Finally, we have looked at the I-V characteristic of the structure in Fig.8e; we assumed that doping of the P-type silicon particle is $10^{17}cm^{-3}$. Then, for various doping concentration of the N-type particle, I-V graphs are obtained. In contrast to the structure in section , here, the short circuit current is significantly influenced by doping; At higher dopings, the short circuit current is reduced to $15.9\frac{mA}{cm^2}$. Although the open circuit voltage is increased, the total power conversion efficiency is reduced and reaches 7%.

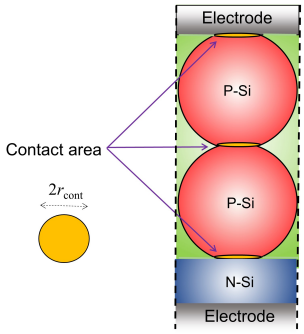

Figure 7. A cell composed of silicon nanoparticles with imperfect shapes. A small volume on top and and below area of each nanoparticle is defined that has a circular cross-section with the radius r_{cont}

.

Geometrical parameters		Silicon		PEDOT:PSS	
d_{N-Si}	300 [nm]	DC Permittivity	11.7	Permittivity	3.8
d_{P-Si}	600 [nm]	$n+i\kappa$	From Palik[35]	Hole mobility	$5\times10^{-4}\text{cm}^2/\text{V.s}$
d_{HTL}	50 [nm]	Sur. Rec. Vel.	vary	Electron affinity	5.1[ev]
W_{cell}	600 [nm]	P-Si Doping	10^{17}cm^{-3}	Bandgap	1.65[ev]
R contact area ($r_{\text{cont.}}$)	60 [nm]	SRH, Rad. Auger Rec.	From[36]	Electron concentration	$2\times10^{18}\text{cm}^{-3}$

Table 1. Geometrical specifications and material properties of the structure shown in Fig.6a.

Impact of SiO_2 nanoparticles

Although the texturing nature of nanoparticles is an effective mean to enhance light trapping in the proposed cell structures, existing a contact layer can slightly reduce this benefit. This is due to the flat structure of these layers as shown in Fig.6a and Fig.8a. One idea to further improve light trapping is to use SiO_2 nanoparticles on top of the cell which has been demonstrated in[37]. Figures 9a and b show the schematic of the structures A and B when SiO_2 nanoparticles are included. In addition, Fig.9a and b show the total photocurrent and the current enhancement as a function of SiO_2 particle size in structures shown in Fig.6a and Fig.8a, respectively. As can be seen, the presence of SiO_2 nanoparticles can enhance the photocurrent in both structures; smaller particles with - with $R_{SiO2} < 300\,\text{nm}$ lead to negligible current enhancement in both cells. As we use larger particles, the current enhancement reaches above 10% at $R_{SiO2} = 500\,\text{nm}$ in the first cell and 8% in the second structure. The sensitivity of enhancement factor to the particle size is due to the interaction of different Mie resonances in SiO_2 and Si nanoparticles.

Discussion

While the physical mechanism for operation and analysis of the described cells is realizing carrier separation via a p-n junction, by using hole transport polymers such PEDOT:PSS in contact with n-type silicon in Fig.6a, a hybrid organic-inorganic junction is also formed. In[38] it is demonstrated that such these contacts act almost like a quasi p-n junction. Based on the free carrier movement in a simple PEDOT:PSS/N-Si junction, the generated carriers in our case studies is expected to constructively contribute in the overall current density. Another issue is about the effect of crystallinity of the silicon nanoparticle. We only considered crystalline silicon particles. Cells based on amorphous silicon nanoparticles despite leading to higher absorption, present weak carrier mobilities and thus, provide poor conversion efficiencies[34]. We assumed that the silicon bandgap is unchanged by doping. At high levels of doping, bandgap narrowing appears which limits the increment of open circuit voltage(see[39]). In addition, we did not consider series resistance in the presented electrical calculations because the main purpose of this work was to propose the conceptual design of the structure without concentrating on a specific contact; Apparently, resistance - which is proportional to the contact material - slightly reduces the fill factor and hence, the cell efficiency. An inevitable consideration about the top contact is to choose materials which prevent diffusion of oxygen to the hole transport medium and silicon particles. This is because emerging oxide layer around the nanoparticles can effect cell performance. Although thin oxide layers (say below 1nm) can help in passivation of dangling bonds on the particle surface, further increase in the thickness prevents their transport between particles.

Concluding remarks

In this paper, we proposed that multi-layer silicon nanoparticles of sub-micron dimensions can be deployed as the absorber of an ultrathin solar cell. We provided a parametric analysis to study the absorption behavior of the stack of these Mie scatterers

$R_{\text{cont.}}$ [nm]	$V_{\text{oc}}[V]$	$J_{\text{sc}}[\frac{\text{mA}}{\text{cm}^2}]$	$\eta\%$
60	0.492	25.24	9.96
40	0.473	12.26	4.36
20	0.472	11.41	4.13

Table 2. Effect of contact area on electrical parameters of the cell shown in Fig.6a. The doping of the silicon layer is assumed to be 10^{17}cm^{-3}.

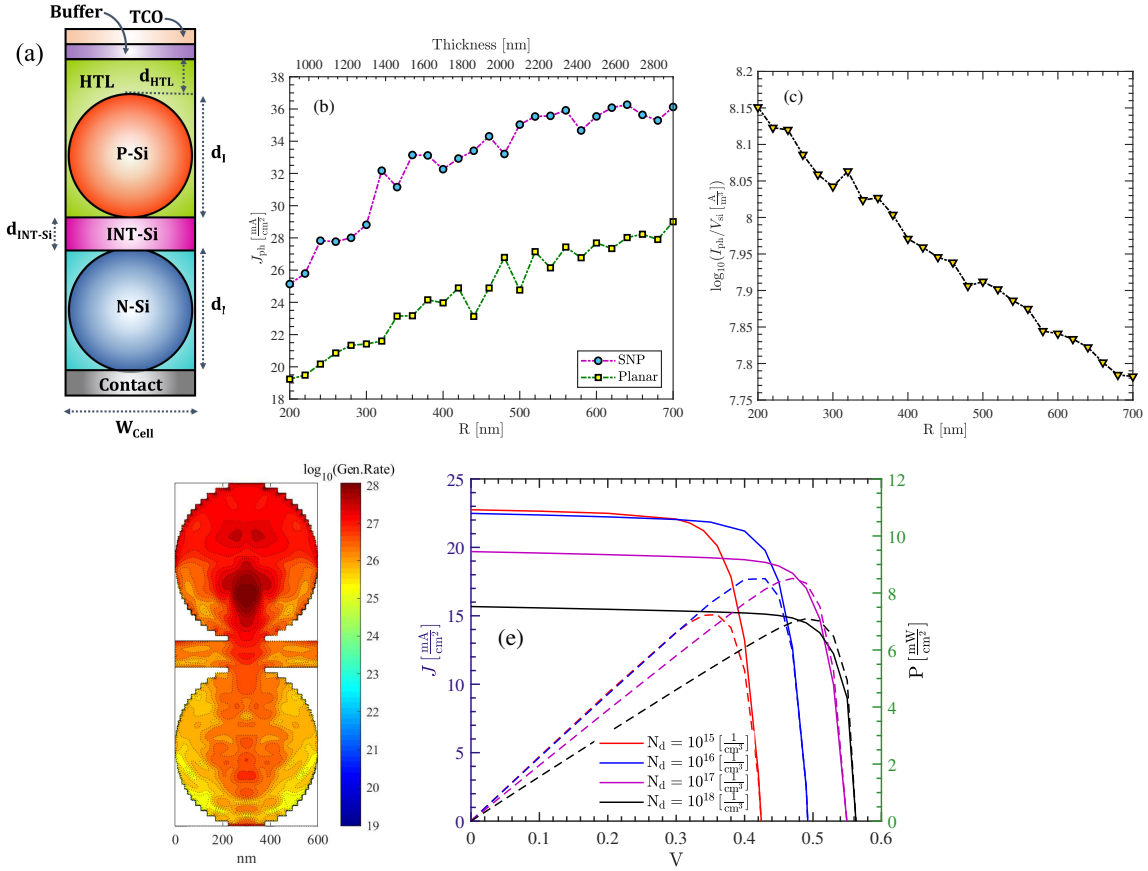

Figure 8. The schematic of the unit cell composed of a p-doped and n doped silicon nanoparticles inside a HTL and ETL material, respectively. The two media are separated by a thin intrinsic silicon layer. The dimensions are listed in Table 3. (b) The photocurrent generated in structure shown in (a), and a conventional cell of identical thickness, as a function of particle size/absorber thickness. (c) The generated current per volume of the absorber for the cell shown in (a), as a function of particle radius. (d) The distribution of the generation rate in the cross-section of the unit cell in a logarithmic representation (unit is in m^{-3}). (e) J-V characteristics of the cell in (a), as a function of doping level of the silicon layer. The electrical parameters of the cell materials are brought in Tabs 1 and 3.

Geometrical parameters		SnO2	
d_{N-Si}	300 [nm]	DC Permittivity	11.7
d_{P-Si}	600 [nm]	$n+i\kappa$	From Palik[35]
d_{HTL}	50 [nm]	Sur. Rec. Vel.	vary
W_{cell}	600 [nm]	P-Si Doping	10^{17}cm^{-3}
R contact area ($r_{\text{cont.}}$)	60 [nm]	SRH, Rad. Auger Rec.	From[36]

Table 3. Geometrical specifications and material properties of the structure shown in Fig.8a.

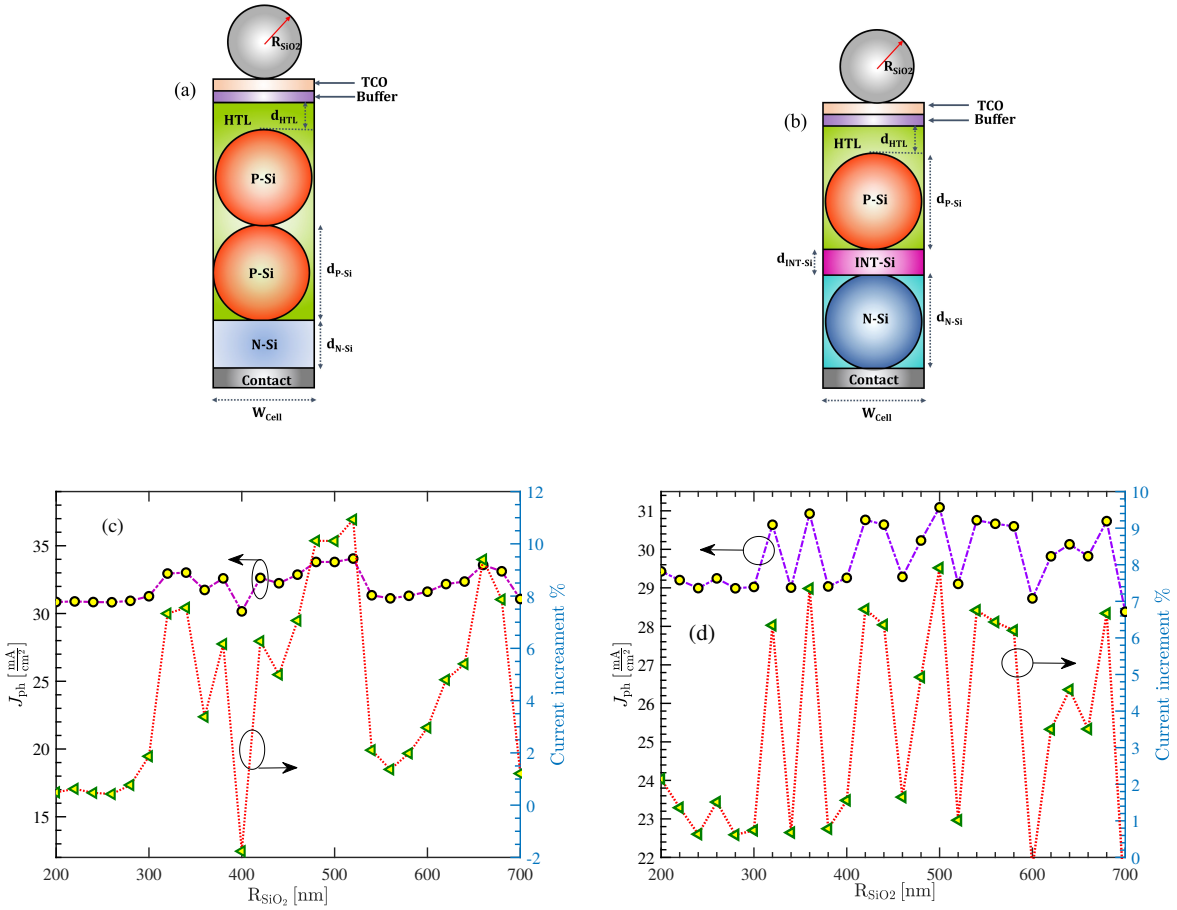

Figure 9. (a) and (b) show the unit cell of the structures A and B, respectively when SiO_2 nanoparticles are added on the top surface. The total photocurrent (dashed-circle line) and current enhancement (dotted-triangle line) in the presence of silica nanoparticles of various dimensions, on top of the structures shown in Figs.6a and 8b. The radius of the silicon particles are assumed to be 300 nm in both (a) and (b). Other geometrical parameters are as those mentioned in Tab.1 and 3.

and showed that the absorption efficiency of the structure is higher at lower number of layers and it approaches to absorption of a flat silicon layer for higher number of layers. We showed that in a dense distribution of silicon nanoparticles, their periodicity play a negligible role in absorption improvement. Several configurations were introduced to tailor these particles as a p-n junction cell. We finally investigated the electrical performance of selected case studies and found that the theoretical efficiency can reach about 11%, which is a promising value for such an ultrathin structure. Moreover, we showed that by including silica nanoparticles of proper size on top of the cell structure, one can enhance the photocurrent up to around 10%.

Methods

In this paper, we numerically investigated the optical performance of the proposed solar cell with multi-layer silicon nano-spheres via full-wave simulation in CST. Due to the resonant nature of a SNP solar cell, we used the FDFD solver to achieve appropriate response accuracy; this solver also allows choosing the number of simulated frequencies in the interested interval. We applied periodic boundary conditions under normally(or obliquely, if needed) propagation of plane wave. The absorbed power inside the silicon parts, together with the corresponding generation rate were calculated. For the electric analysis, we then simulate the 3D cell structures in the Charge module of Lumerical. For this, each sphere was modeled as a stack of 3D polygons having thin thicknesses. The obtained generation rate is imported in the simulation. In addition, the material properties including permittivities, dopings and losses found in the literature were considered for silicon, silver and polymer parts.

Acknowledgements

Authors acknowledge support from the University of Tehran, Science and Technology park.

Author contributions statement

S. R. M and M. A. Sh. performed calculations and simulations as well as the analysis. L.Y. guided the research. All authors reviewed the manuscript.

Additional Information

Competing Interests: The authors declare no competing interests.

Data Availability

The datasets generated during and/or analysed during the current study are available from the corresponding author on reasonable request.

References

1. Wang, S. *et al.* Large-area free-standing ultrathin single-crystal silicon as processable materials. *Nano letters* **13**, 4393–4398 (2013).
2. Sayre, L. *et al.* Ultra-thin photovoltaics for radiation-tolerant space power systems. In *Physics, Simulation, and Photonic Engineering of Photovoltaic Devices X*, vol. 11681, 1168106 (International Society for Optics and Photonics, 2021).
3. Abad, E. C., Joyce, H. J. & Hirst, L. C. Light management in ultra-thin solar cells: a guided optimisation approach. *Opt. Express* **28**, 39093–39111 (2020).
4. Massiot, I., Cattoni, A. & Collin, S. Progress and prospects for ultrathin solar cells. *Nat. Energy* **5**, 959–972 (2020).
5. Ingenito, A., Isabella, O. & Zeman, M. Experimental demonstration of 4 n 2 classical absorption limit in nanotextured ultrathin solar cells with dielectric omnidirectional back reflector. *ACS photonics* **1**, 270–278 (2014).
6. Ferry, V. E. *et al.* Light trapping in ultrathin plasmonic solar cells. *Opt. express* **18**, A237–A245 (2010).
7. Scanlon, D. O. & Walsh, A. Bandgap engineering of znsnp2 for high-efficiency solar cells. *Appl. Phys. Lett.* **100**, 251911 (2012).
8. Todorov, T. *et al.* Monolithic perovskite-cigs tandem solar cells via in situ band gap engineering. *Adv. Energy Mater.* **5**, 1500799 (2015).
9. McIntosh, K. R., Altermatt, P. P. & Heiser, G. Depletion-region recombination in silicon solar cells: when does mdr= 2. In *Proceedings of the 16th European photovoltaic solar energy conference*, 251–254 (2000).
10. Kerr, M. J., Cuevas, A. & Campbell, P. Limiting efficiency of crystalline silicon solar cells due to coulomb-enhanced auger recombination. *Prog. Photovoltaics: Res. Appl.* **11**, 97–104 (2003).
11. Yu, K. J. *et al.* Light trapping in ultrathin monocrystalline silicon solar cells. *Adv. Energy Mater.* **3**, 1401–1406 (2013).
12. Shameli, M. A. & Yousefi, L. Absorption enhanced thin-film solar cells using fractal nano-structures. *IET Optoelectronics* **15**, 248–253 (2021).
13. Shameli, M. A., Fallah, A. & Yousefi, L. Developing an optimized metasurface for light trapping in thin-film solar cells using a deep neural network and a genetic algorithm. *JOSA B* **38**, 2728–2735 (2021).
14. Shameli, M. A., Mirnaziry, S. R. & Yousefi, L. A thin-film sis solar cell based on distributed silicon nanoparticles. In *2021 29th Iranian Conference on Electrical Engineering (ICEE)*, 816–820 (IEEE, 2021).
15. Gruginskie, N. *et al.* Increased performance of thin-film gaas solar cells by rear contact/mirror patterning. *Thin Solid Films* **660**, 10–18 (2018).
16. Goffard, J. *et al.* Light trapping in ultrathin cigs solar cells with nanostructured back mirrors. *IEEE journal photovoltaics* **7**, 1433–1441 (2017).
17. Wang, K. X., Yu, Z., Liu, V., Cui, Y. & Fan, S. Absorption enhancement in ultrathin crystalline silicon solar cells with antireflection and light-trapping nanocone gratings. *Nano letters* **12**, 1616–1619 (2012).

18. Abass, A., Le, K. Q., Alu, A., Burgelman, M. & Maes, B. Dual-interface gratings for broadband absorption enhancement in thin-film solar cells. *Phys. Rev. B* **85**, 115449 (2012).

19. Le, K. Q., Abass, A., Maes, B., Bienstman, P. & Alù, A. Comparing plasmonic and dielectric gratings for absorption enhancement in thin-film organic solar cells. *Opt. express* **20**, A39–A50 (2012).

20. Jovanov, V. *et al.* Influence of interface morphologies on amorphous silicon thin film solar cells prepared on randomly textured substrates. *Sol. Energy Mater. Sol. Cells* **112**, 182–189 (2013).

21. Shameli, M. A. & Yousefi, L. Light trapping in thin film crystalline silicon solar cells using multi-scale photonic topological insulators. *Opt. & Laser Technol.* **145**, 107457 (2022).

22. Gao, Q. *et al.* A novel metal precursor structure for electrodepositing ultrathin cigse thin-film solar cell with high efficiency. *ACS applied materials & interfaces* **12**, 24403–24410 (2020).

23. Mellor, A. *et al.* Nanoparticle scattering for multijunction solar cells: the tradeoff between absorption enhancement and transmission loss. *IEEE J. Photovoltaics* **6**, 1678–1687 (2016).

24. Yao, Y. *et al.* Broadband light management using low-q whispering gallery modes in spherical nanoshells. *Nat. communications* **3**, 1–7 (2012).

25. Estakhri, N. M. & Alu, A. Physics of unbounded, broadband absorption/gain efficiency in plasmonic nanoparticles. *Phys. Rev. B* **87**, 205418 (2013).

26. Yu, P. *et al.* Giant optical pathlength enhancement in plasmonic thin film solar cells using core-shell nanoparticles. *J. Phys. D: Appl. Phys.* **51**, 295106 (2018).

27. Furasova, A. *et al.* Engineering the charge transport properties of resonant silicon nanoparticles in perovskite solar cells. *Energy Technol.* **8**, 1900877 (2020).

28. Eyderman, S., Deinega, A. & John, S. Near perfect solar absorption in ultra-thin-film gaas photonic crystals. *J. Mater. Chem. A* **2**, 761–769 (2014).

29. Kazerooni, H. & Khavasi, A. Plasmonic fractals: ultrabroadband light trapping in thin film solar cells by a sierpinski nanocarpet. *Opt. Quantum Electron.* **46**, 751–757 (2014).

30. Matson, R. J., Emery, K. A. & Bird, R. E. Terrestrial solar spectra, solar simulation and solar cell short-circuit current calibration: a review. *Sol. cells* **11**, 105–145 (1984).

31. Luo, J.-W., Stradins, P. & Zunger, A. Matrix-embedded silicon quantum dots for photovoltaic applications: a theoretical study of critical factors. *Energy & Environ. Sci.* **4**, 2546–2557 (2011).

32. Baranov, D. G. *et al.* All-dielectric nanophotonics: the quest for better materials and fabrication techniques. *Optica* **4**, 814–825 (2017).

33. Shameli, M. A., Mirnaziry, S. R. & Yousefi, L. Distributed silicon nanoparticles: an efficient light trapping platform toward ultrathin-film photovoltaics. *Opt. Express* **29**, 28037–28053 (2021).

34. Ding, Y. *et al.* Optical, electrical, and photovoltaic properties of silicon nanoparticles with different crystallinities. *Appl. Phys. Lett.* **107**, 233108 (2015).

35. Palik, E. D. *Handbook of optical constants of solids*, vol. 3 (Academic press, 1998).

36. Markvart, T., McEvoy, A. *et al. Practical handbook of photovoltaics: fundamentals and applications* (Elsevier, 2003).

37. Grandidier, J. *et al.* Solar cell efficiency enhancement via light trapping in printable resonant dielectric nanosphere arrays. *physica status solidi (a)* **210**, 255–260 (2013).

38. Jäckle, S. *et al.* Junction formation and current transport mechanisms in hybrid n-si/pedot: Pss solar cells. *Sci. reports* **5**, 1–12 (2015).

39. Zerga, A., Benosman, M., Dujardin, F., Benyoucef, B. & Charles, J. New coefficients of the minority carrier lifetime and bandgap narrowing models in the transparent emitter of thin film silicon solar cells. *Active passive electronic components* **26**, 1–10 (2003).